Up and down cascade in a dynamo model: Spontaneous symmetry breaking

E. M. Blanter,[1,2] C. Narteau,[2] M. G. Shnirman,[1,2] and J.-L. Le Mouël[2]
[1]*International Institute of Earthquake Prediction Theory and Mathematical Geophysics, Warshavskoye sh 79, Korp 2, Moscow 113556, Russia*
[2]*Institut de Physique du Globe de Paris, 4 Place Jussieu, 75252 Paris Cedex 05, France*
(Received 6 April 1998; revised manuscript received 20 November 1998)

A multiscale turbulent model of dynamo is proposed. A secondary magnetic field is generated from a primary field by a flow made of turbulent helical vortices (cyclones) of different ranges, and amplified by an up and down cascade mechanism. The model displays symmetry breakings of different ranges although the system construction is completely symmetric. Large-scale symmetry breakings for symmetric conditions of the system evolution are investigated for all kinds of cascades: pure direct cascade, pure inverse cascade, and up and down cascade. It is shown that long lived symmetry breakings of high scales can be obtained only in the case of the up and down cascade. The symmetry breakings find expression in intervals of constant polarity of the secondary field (called chrons of the geomagnetic field). Long intervals of constant polarity with quick reversals are obtained in the model; conditions for such a behavior are investigated. Strong variations of the generated magnetic field during intervals of constant polarity are also observed in the model. Possible applications of the model to geodynamo modeling and various directions of future investigation are briefly discussed. [S1063-651X(99)10605-6]

PACS number(s): 05.40.−a, 91.25.Cw, 47.65.+a

I. INTRODUCTION

Current observations at the surface of the Earth show that there exists a geomagnetic field that is grossly the field of a dipole located at the Earth's center and inclined by 11° (today) on the Earth's rotation axis. The difference between the observed magnetic field and the dipole one—the nondipole field—is about 10% in relative root mean square value. There exist three kinds of observations that give us information about the time evolution of the geomagnetic field: direct measurements, which do not go back beyond three centuries [1], archeomagnetic data (the past magnetic field is fossilized in artifacts like baked clays), and paleomagnetic data (the ancient field is fossilized in sedimentary and volcanics rocks). Direct measurements show that the time constant of the nondipole field is of the order of two hundred years [2]; the time constant of the equatorial part of the dipole, as inferred from archeomagnetic data, is rather of the order of a few hundreds years [3].

The present paper is devoted to the behavior of the geomagnetic field over geological times; time constants of a few hundred years are smoothed out. Paleomagnetic data first show that, when averaged on a few thousands of years, the geomagnetic field is indeed the field of an axial dipole (in agreement of the above time constant), i.e., aligned along the rotation axis. But, when considering longer time spans, of millions to hundreds of millions of years, it comes out that the polarity of this axial dipole changes in time, going from North-South to South-North and vice versa. These are the so-called reversals of the geomagnetic field. Periods between reversals are called polarity intervals, or chrons. The duration of polarity intervals have changed during geological times [4]. For example, since 80 million years (Myr) ago, it has (in average) decreased from about 1 Myr to 0.2 Myr. The duration of the reversals [typically 4 or 5 thousands of years (kyr)] is quite short compared to the duration of the polarity intervals. Sometimes, very long polarity intervals occur, as the cretaceous superchron, which extends from 118 to 83 Myr before present. As for the intensity of the dipole, it displays strong temporal variations during a chron.

In the present paper we will focus on the reversals process and the succession of polarity intervals.

The origin of the Earth's magnetic field is probably the most outstanding problem of geophysics. Some basic properties of the core of the Earth may be evaluated: the conductivity of the core iron is about $10^6\ (\Omega\,\mathrm{m})^{-1}$, the velocity of the flow stirring the fluid is of the order of $10^{-3}\ \mathrm{ms}^{-1}$, as inferred from the temporal (secular) variation of the geomagnetic field measured at the Earth's surface; the corresponding magnetic Reynolds number is $\sim 10^2$. Due, in particular, to this high value, it is generally believed that the origin of the Earth's magnetic field is an autoexcited dynamo process at work in the metallic fluid core of the planet.

A considerable amount of work has been devoted to geodynamo theory. A well-known approach consists in the so-called $\alpha\omega$ and α^2 dynamo models; in a somewhat loose way we will refer to this theory in our model. The magnetic field inside the core is the sum of a poloidal ingredient, with a radial component, whose field lines escape the core, and of a toroidal ingredient whose field lines are horizontal and which is then confined inside the core. A differential rotation of the core layers, attributed to convection and transfer of angular momentum, is called for to generate—through the winding of the magnetic field lines around the rotation axis—a toroidal magnetic field from a poloidal one. The mechanism is called ω effect. Unfortunately it cannot work in the reverse way. It is resorted to the so called α effect [5–7]: a turbulent small scale motion, nonmirror symmetric, generates, as shown by a mean field theory [7], a poloidal ingredient from a toroidal one, and conversely. It is important to emphasize that the turbulent motion must be nonmirror symmetric, its

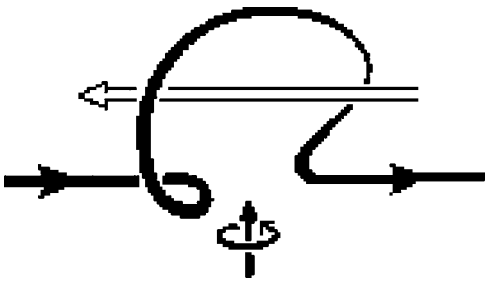

FIG. 1. A flux rope twisted into a Ω by a right handed motion. The loop is accompanied by an electric current antiparallel to the magnetic field (after Krause and Rädler, Ref. [7]).

helicity $\alpha = -\vec{u}\cdot\vec{\nabla}\times\vec{u}$, averaged in a certain large scale domain, is not zero. Figure 1 shows schematically the effect of an elementary helical motion (a cyclone, right-handed in the figure case, $\alpha<0$) on a large scale magnetic field, the mechanism at the base of α effect. As a result, a flow made of a large scale differential rotation and a small scale turbulent helical flow can maintain the magnetic field against ohmic dissipation; this is the $\alpha\omega$ dynamo. But, as said above, the α effect can as well build a toroidal ingredient from a poloidal one, and can work alone; this is the α^2 dynamo. Energy is provided by the cooling of the Earth and the corresponding increase of the solid inner core, giving raise to thermal or/and compositional convection. In nearly axisymmetric $\alpha\omega$ dynamos [8–13] $\alpha(\vec{x})$ is given, $\vec{x}$ being the current point in the core. For example, it is often assumed that $\alpha\sim\cos\Theta$, Θ being the colatitude; helicity has different signs in the two hemispheres.

Of course, instead of computing these parametrical models, in which only some global effect of the mechanisms at work is considered, one can try to solve numerically directly the magnetohydrodynamic equations. Indeed, impressive numerical codes have been recently built which have given spectacular results [14,15]. In particular, reversals are observed, although their mechanism and meaning are not yet well understood. Nevertheless these computations, however complex, cannot be performed for realistic values of the involved parameters, in particular the viscosity. The effect of viscosity in the rotating core is characterized by the Ekman number $E=\nu/2\Omega a^2$, ν being the kinematic viscosity of the core fluid, Ω the Earth's rotation, a the core radius. The value of E for the Earth's core is probably typically 10^{-15}, whereas the (hyperviscous) numerical models cannot handle Ekman numbers smaller than 10^{-6}. It is possible that it is not necessary to go down to values of E as small as 10^{-15} to reach the asymptotic regime of the numerical models. In any case, due to this small viscosity, the Reynolds number of the core fluid is of the order of 10^8, and a turbulent flow is expected which cannot be described by the numerical codes.

In the present work, instead of the small scale turbulence postulated in $\alpha\omega$ and α^2 dynamos, we will consider a fully developed turbulence, or rather a simplified model of fully developed turbulence in the form of a multiscale helical motion. This multiscale motion is assumed to generate, in presence of a primary large scale magnetic field, a secondary large scale magnetic field. Multiscale turbulence is associated with a direct cascade of energy [16–19]; therefore a direct cascade is part of the present model of dynamo. On the other hand, scaling properties of the turbulence govern the hierarchical structure of the model. An inverse cascade results of the generation of structures of higher ranges through the electromagnetic interaction of lower ranges structures.

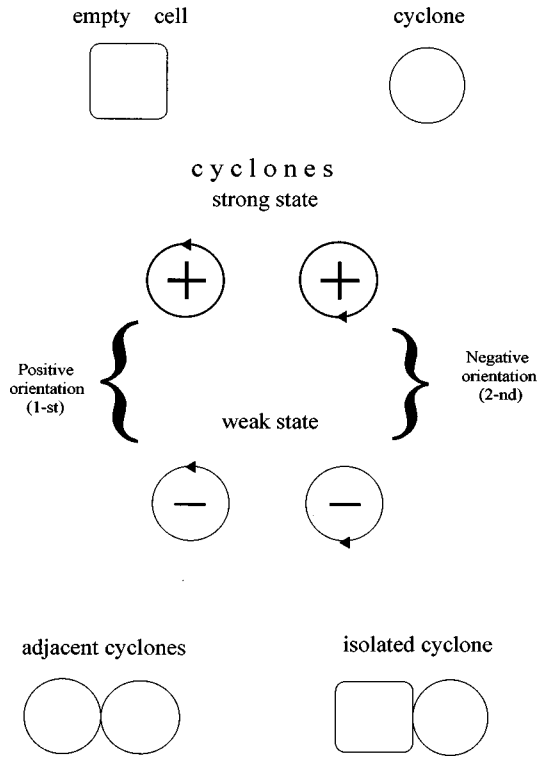

FIG. 2. Properties of vortices.

Such a hierarchical model of dynamo, with an inverse cascade as a main ingredient (but without direct cascade and with a weakly nonmirror symmetric generation mechanism), was already investigated in [20] where differential rotation was also considered to build a kind of $\alpha'\omega$ dynamo, although a very schematic one. The same kind of hierarchical structure and inverse cascade mechanism had been applied previously to modeling seismicity and crack propagation [21–27].

Physical assumptions determining the general construction of the model are presented in Sec. II. Section III contains a general description of the model; basic notions and definitions are given in Sec. III A and Sec. III B contains the complete description of all the steps of the system evolution. Properties and conditions for symmetry breaking are investigated in Sec. IV. Possible applications and general directions of future investigations are discussed in Sec. V.

II. BASIC NOTIONS

We consider, as said above, a multiscale turbulent motion in a conducting fluid pervaded by a primary magnetic field. Our model, rather abstract, is made of helical vortices (or cyclones) of different embedded scales; a vortex of level l occupies a cell of level l of a hierarchically organized system of cells (see Sec. 3 and Fig. 2). We therefore consider localized vortices interacting together. Interaction of localized vortices, especially point vortices, in fluid dynamics and magnetohydrodynamics, is a time honored subject. Discrete vortex representations are described in [28–30]. These rep-

resentations give raise to an elegant Hamiltonian formalism [31–33]. The formalism we adopt here is more phenomenological, with a less strong mathematical and physical basis, but we systematically resort to renormalization methods to derive the general properties of our model. We attribute interactions between vortices mainly to electromagnetic effects, although keeping again a phenomenological point of view. The study of the magnetohydrodynamics (MHD) of a helical flow can be found in [34]; fully developed MHD turbulence has been considered in [35,36].

Let us now describe the general features of our model. The helical vortices (cyclones) can be right-handed or left-handed, we will say can have two orientations, 1 and 2 (our vortices are not at all 2D vortices; they are simplified representations of 3D cyclonic structures). The interaction of an helical motion with the existing magnetic field produces an electric current parallel or antiparallel to the applied primary magnetic field, depending on its orientation [5] (see Fig. 1); a secondary magnetic field results. Let us say that the vortices of the first orientation give a positive contribution to the magnetic field, the vortices of the second orientation a negative one. Globally, the intensity and sign of the secondary magnetic field depend on the number, scales and orientations of the vortices involved in the turbulent motion.

It is assumed that the turbulence generates vortices of both orientations, and sustains their existence during a random time interval. A mirror symmetry of the turbulence generation is postulated: vortices of orientation 1 and vortices of orientation 2 appear with the same probability. To respect this symmetry, the evolution of vortices of both orientations is ruled by the same parameters of the model. In $\alpha\omega$ or α^2 models, as said earlier, it is assumed a priori that the turbulence is not mirror-symmetric, and the expression of the helicity is given (e.g, $\alpha \sim \cos\Theta$). The lack of symmetry and the change of sign of α from an hemisphere to the other are attributed in these models to the Earth's rotation. Nevertheless, ''insofar as homogeneous isotropic turbulence exists in nature, it is difficult to find convincing reasons for such turbulence to be nonmirror symmetric'' [7]. In the present model, the generation of turbulence is supposed mirror symmetric, but spontaneous symmetry breakings will occur, leading to large scale lacks of mirror symmetry. This is the very subject of the paper.

The temporal evolution of a vortex is governed by a continuously increasing instability which eventually leads to its destruction. The increase of the vortices instability can be viewed as a relaxing process in the course of which the vortices properties change continuously; for the sake of simplicity, we introduce a discretization of the relaxing process: two living states of the vortices (strong and weak) are considered (Fig. 2). The strong living state is characteristic of a vortex soon after its appearance; the weak state is characteristic of a vortex before its destruction. Destroying a vortex produces its disintegration into vortices of similar orientation and lower ranges. The disintegration process generates a direct cascade of energy transfer similar to the turbulent cascade (Fig. 3).

Interactions between vortices are governed by repulsion (attraction) of antiparallel (parallel) electric currents generated by these vortices in the magnetic field. Two basic kinds of interaction between vortices of same range are considered:

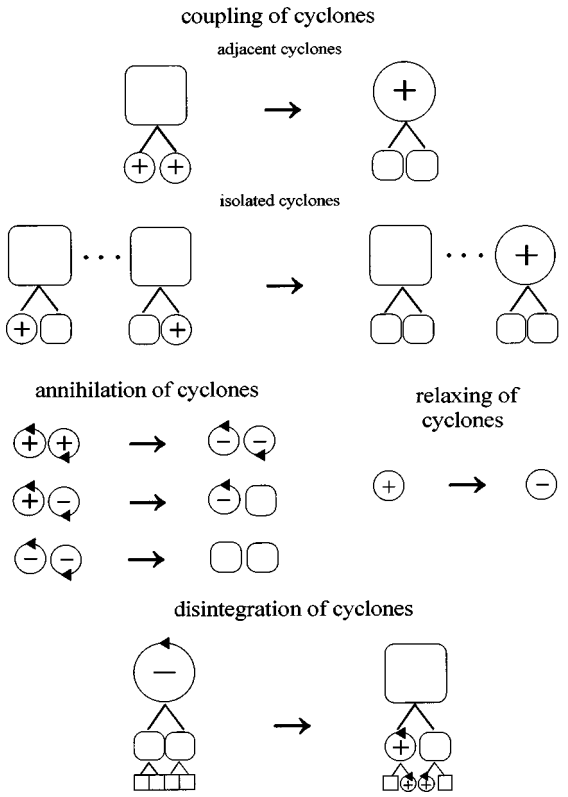

FIG. 3. Basic transformations of vortices.

vortices with the same orientation attract one another and can couple; vortices with opposite orientation located nearby one another can annihilate each other (Fig. 3). The coupling process transforms two coupling vortices into one vortex of higher range and generates an inverse cascade. The annihilation process amplifies the instability of interacting vortices: it changes strong living states into weak living states, or destroys weak vortices (Fig. 3).

The evolution of the vortices governs the evolution of the secondary magnetic field which they generate. The sign of the secondary magnetic field is determined mainly by the orientation of the vortices of high ranges. When there is a balance between the two opposite orientations of vortices of high ranges, the intensity of the secondary magnetic field is close to zero. A sufficient symmetry breaking in the vortices orientations is needed to generate a magnetic field with a significantly nonzero intensity. This symmetry breaking must last long enough, and quick transitions from one polarity to the opposite one must occur, if we wish to mimic the behavior of the geomagnetic field. The problem of the generation of a large scale secondary magnetic field with polarity intervals and reversals reduces to the investigation of large scale symmetry breakings in the evolution of the vortices.

III. MODEL DESCRIPTION

A. Basic definitions of the model

Properties of vortices

Scaling properties of the turbulence govern the hierarchical construction of the model. It is assumed that the vortices of different scales appear in hierarchically organized cells (Fig. 4); if two vortices of level l occupy one cell of higher

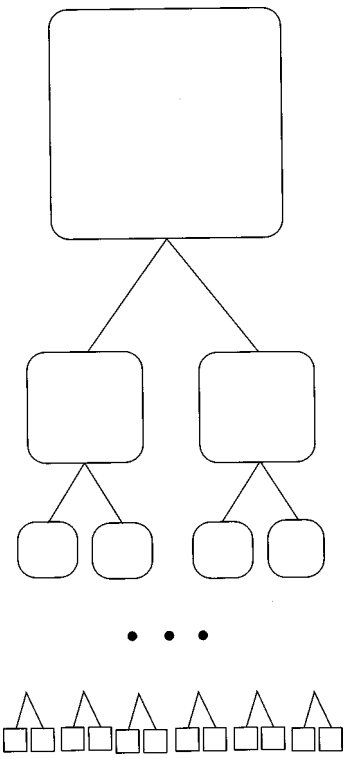

FIG. 4. Hierarchical multiscale structure of cells.

level $(l+1)$, these vortices are referred to as adjacent. If a vortex has no adjacent vortex, it is referred to as isolated (Fig. 2). According to the physical assumptions summarized in the previous section, each vortex has an orientation (1st or 2nd) which remains unchanged as long as it exists in either living state (strong or weak) (Fig. 2). New vortices appear in the strong living state (denoted as $[+]$ vortices), and the strong living state randomly transfers into the weak living state (denoted as $[-]$). Only vortices in the weak living state can be disintegrated.

Relaxing of vortices

The process of transformation of the living state from strong to weak is referred to as the relaxing process (Fig. 2).

Disintegration of vortices

Weak vortices can be randomly disintegrated at each time moment. A vortex of level l disintegrating at time $(t-1)$ disappears at this level and contributes to the appearance at time t of new vortices at all levels lower than l (Fig. 3).

Interactions of vortices

As said above, one assumes two kinds of interaction between vortices of same level: coupling of strong vortices with the same orientation, and annihilation of adjacent vortices with opposite orientations (Fig. 3).

Coupling of vortices. Two strong vortices of level l may be coupled if they have similar orientations; the probability of coupling of two vortices is different depending on wether they are adjacent or not. The coupling of vortices leads to a transition from level l to level $l+1$: the two coupled vortices of level l disappear, and a new vortex of the same orientation appears at level $l+1$ (Fig. 3). Two kinds of coupling are distinguished: coupling of two adjacent vortices and coupling of two isolated vortices. The coupling of adjacent vortices leads to a construction of the inverse cascade similar to the one described in [20,21,23–25,27]. The coupling of isolated vortices was not considered in previous models of inverse cascade; it reflects the possible displacement of isolated vortices in the liquid.

Annihilation of vortices. Two adjacent vortices with opposite orientations may annihilate, which leads to the transformation of strong living states into weak ones and to the disappearance of weak vortices (Fig. 3). Disappearance of vortices by annihilation is not equivalent to disintegration of vortices and does not contribute to the appearance of new vortices of lower ranges.

Recapitulation

Let us now recapitulate how vortices appear and disappear.

Appearance of new vortices. There are therefore three different causes for appearance of new vortices of a given range l: generation by the permanent turbulent motion, coupling of vortices of lower levels, and disintegration of vortices of higher levels.

(a) It is assumed that the turbulence generates continuously new vortices at all levels of the system. This contribution to the appearance probability does not depend on the orientation of the appearing vortex (mirror symmetry of the generation mechanism).

(b) Coupling of two strong vortices of level l leads to the appearance of a new vortex at level $l+1$. Globally, the coupling process produces an inverse cascade from lower to higher levels of the system.

(c) Weak vortices of level higher than l which have disintegrated at time $t-1$ contribute to the appearance of new vortices of level l at time t. Globally, the disintegration process produces a direct cascade from higher to lower levels of the system.

Disappearing of vortices. There are therefore three different ways for vortices to disappear at a given level in the model (Fig. 3).

(a) Disintegration of weak vortices. New vortices appear at lower levels at the next time moment.

(b) Coupling of strong vortices of level l leads to the disappearing of the coupling vortices at level l and to the appearing of new vortices at the higher level (see supra).

(c) Annihilation of a weak vortex with an adjacent one of the opposite orientation. No new vortex appears in this case.

Generation of the magnetic field

We choose the intensity of the secondary magnetic field as a global parameter characterizing the evolution of the model. All vortices existing at time t contribute additively to the intensity of the secondary magnetic field generated at this time. The contribution of a vortex increases with its level. The sign of the contribution depends on the orientation of the vortex: vortices of the first orientation make a positive contribution; vortices of the second orientation a negative one.

B. Temporal evolution of the system

For computational reasons, it is assumed that all the processes described above take place consecutively in time dur-

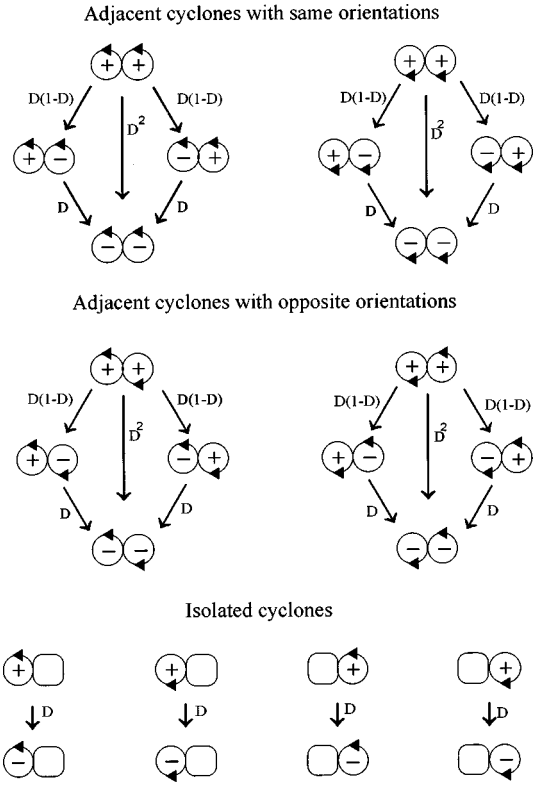

FIG. 5. Relaxing of [+] vortices. The arrows denote possible transformations of vortices with the probability indicated nearby. For vortices of level l, the value of D is equal to the probability of relaxing $D(l)$.

ing one time step of the modeling. The following sequence of state transformations at level l is assumed during one time step: relaxing of vortices; annihilation of adjacent vortices with opposite orientations; disintegration of vortices; direct cascade of appearance of new vortices; inverse cascade of appearance of new vortices; disappearing of coupling vortices.

We give below a detailed description of these transformations, expliciting quantitatively the features of the model qualitatively described earlier.

Relaxing of [+] vortices

The relaxing process is the transformation of strong vortices into weak ones (Fig. 3). A [+] vortex of level l transforms into a [−] vortex of level l with probability $D(l)$. This probability does not depend on the orientation of the vortex, and does not change with time. It is expressed as follows:

$$D(l)=D_0\delta^l, \quad \delta<1. \tag{1}$$

The scaling relationship between the relaxing probability $D(l)$ and the level l of the vortex accounts for the property of vortices of higher levels to keep longer their strong state; the relaxing probability $D(l)$ is indeed inversely proportional to the average lifetime of a [+] vortex of level l. All possible state transitions of a pair of adjacent elements are presented on Fig. 5. Each arrow indicates a possible transition of a pair between two states, with the corresponding probability indicated nearby. A given pair keeps its current state with a probability which is the complement to 1 of the sum of all

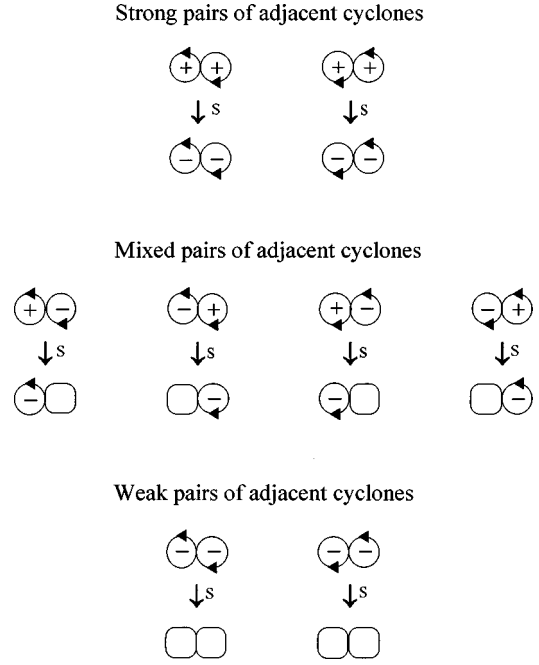

FIG. 6. Annihilation of adjacent vortices with opposite orientations. The arrows denote possible transformations of vortices with the probability indicated nearby. For vortices of level l, the value of S is equal to the probability of annihilation $S(l)$.

the transition probabilities possible for the given state. The state of pairs of adjacent elements which are not displayed on Fig. 5 does not change during this relaxing time substep.

Annihilation of mixed pairs

Two adjacent vortices of level l with opposite orientations annihilate each other with probability $S(l)$. This probability is constant in time, does not depend on the states [+] or [−] of the vortices, and respects the higher stability of vortices of higher levels:

$$S(l)=S_0\sigma^l, \quad \sigma<1. \tag{2}$$

For strong vortices the annihilation means transition to the weak state, for weak vortices it means the disappearing of the vortex (Fig. 3). Possible transformations of a pair of adjacent vortices with opposite orientations are presented on Fig. 6. The kinds of pairs which are not displayed on Fig. 6 remain unchanged during this annihilation substep.

Disintegration of [−] vortices

Disintegration of weak vortices of level l into vortices of lower levels results in the disappearing of [−] vortices at level l and appearing of new vortices with the same orientation at all levels smaller than l (Fig. 3). Weak vortices of level l disappear with a probability $\beta(l)$ invariant in time and independent of the vortices orientation:

$$\beta(l)=\beta_0 b^l. \tag{3}$$

The lifetime of weak vortices is inversely proportional to the disappearing probability $\beta(l)$. Larger scale vortices have a longer lifetime, and formula (3) accounts for this scaling property.

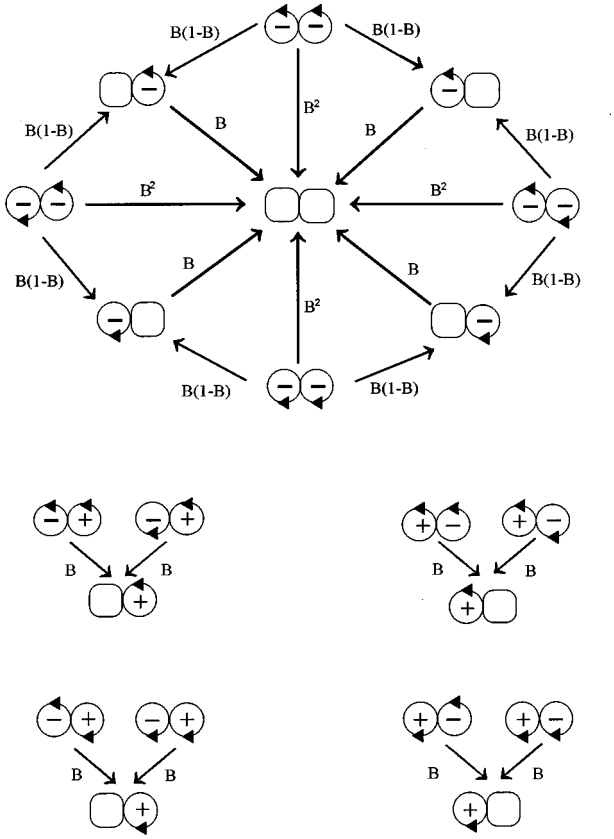

FIG. 7. Disintegration of [−] vortices. The arrows denote possible transformations of vortices with the probability indicated nearby. For vortices of level l, the value of B is equal to the probability of disintegration $\beta(l)$.

All possible state transitions for a pair of adjacent elements at this disintegration substep are presented in Fig. 7. The state of the pairs not present in Fig. 7 remains unchanged.

Densities of disintegrating vortices of ith direction at level l and time t are

$$r_i(l,t)=p_i^-(l,t)\beta(l), \tag{4}$$

where $p_i^-(l,t)$ denotes the density of weak vortices of ith orientation ($i=1,2$) at l level and time t.

Direct cascade of appearance

Direct cascade of appearance of new vortices is generated by two processes: the appearance regularly generated by the turbulence, and the appearance due to the disintegration of [−] vortices of higher levels at the previous time moment $(t-1)$. The helicity flow of range l and ith orientation, at time t, is determined by a functional $E_i(l,t)$ expressed as follows:

$$E_i(l,t)=E_0\varepsilon^l+F_0\sum_{\lambda=l+1}^{L} r_i(\lambda,t)q^{\lambda-l}, \tag{5}$$

where E_0 characterizes the efficiency of the turbulence, the same for both orientations, $r_i(\lambda,t)$ $(i=1,2)$ denotes the densities of vortices of level λ disintegrated at the previous time moment $(t-1)$ [Eq. (4)]. F_0 characterizes the intensity of the disintegration process. Parameters ε and q determine the scaling relationships between the different levels. To obtain an effective cascade effect the scaling parameter q must be chosen larger than unity.

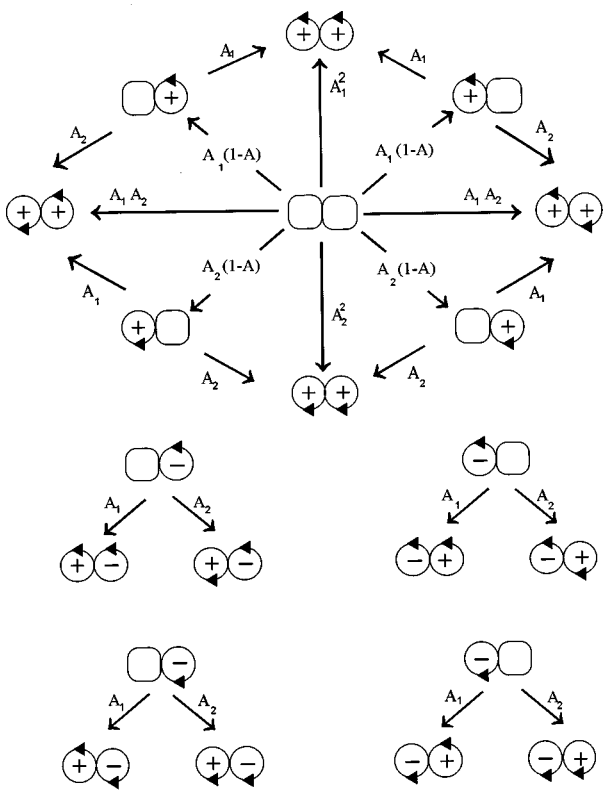

FIG. 8. Appearance of new vortices. The arrows denote possible transformations of vortices with the probability indicated nearby. If the direct cascade of appearance is considered, then for vortices of level l at time t, values of A_i $(i=1,2)$ are equal to the appearance probabilities $A_i(l,t)$; the value A is equal to $A(l,t)$. If the inverse cascade of appearance is considered, then for vortices of level l at time t, values of A_i $(i=1,2)$ are equal to the appearance probabilities $a_i(l,t)/[a_1(l,t)+a_2(l,t)]$; the value A is equal to $a_1(l,t)+a_2(l,t)$.

The probability to obtain a new [+] vortex at level l, regardless to its orientation, is then taken as

$$A(l,t)=1-\exp\{-[E_1(l,t)+E_2(l,t)]\}. \tag{6}$$

The number of vortices of ith direction among all the new vortices of level l appearing at time t is proportional to $E_i(l,t)$; in other words, the relative density of new vortices of ith direction is

$$A_i(l,t)=\frac{E_i(l,t)}{E_1(l,t)+E_2(l,t)}A(l,t), \quad i=1,2. \tag{7}$$

All possible state transitions for a pair of adjacent elements corresponding to this substep are presented in Fig. 8. The state of other pairs does not change during this substep. On the plot A denotes the appearance probability $A(l,t)$ and A_i probabilities $A_i(l,t)$, $(i=1,2)$.

Inverse cascade of appearance

There are two cases of coupling of strong vortices of the same level l (Fig. 3): two adjacent vortices with similar orientations couple with probability $\alpha(l)$, two isolated vortices with similar orientations couple with probability $\gamma(l)$. Coupling probabilities are invariant in time, do not depend on the orientation of the coupling vortices, and increase with the level l as follows:

$$\alpha(l)=\alpha_0\mu^l, \tag{8}$$

$$\gamma(l)=\gamma_0 g^l. \tag{9}$$

Cyclones coupling at level l make a new vortex appear at the superior level $l+1$. The appearance probability of a new vortex of level $l+1$ depends on the density of coupling pairs as follows:

$$a_i(l+1,t)=P_{ii}^{++}(l,t)\alpha(l)+P_i^{+}(l,t)^2\gamma(l), \tag{10}$$

where $i=1,2$ denotes again the orientation of the appearing vortex; $P_{ii}^{++}(l,t)$ and $P_i^{+}(l,t)$ denote respectively the densities of adjacent and isolated active vortices of range l at time t.

All possible state transitions for a pair of adjacent elements at this substep of the computation are presented in Fig. 8. Now A denotes the total probability of appearing of a new vortex, i.e., $a_1(l,t)+a_2(l,t)$; A_i denotes $a_i(l,t)/[a_1(l,t)+a_2(l,t)]$ and represents the relative density of vortices of ith orientation among all the new vortices appearing at this substep ($i=1,2$).

Disappearing of [+] vortices

Strong vortices of level l coupling at time t generate a new vortex at level $l+1$ (as detailed above) and disappear from level l (Fig. 3). The density of coupling pairs disappearing at level l is given by formula (10). Cyclones of the highest level L of the system cannot generate a vortex of superior level, therefore there is no disappearance at the highest level L. The disappearance of coupling vortices at a given level has a physical meaning similar to that of the defects healing mechanism described in [24]: a transition of perturbation from lower to higher levels of the system.

TABLE I. Common parameters of secondary magnetic field generation for Figs. 9–13.

Number of levels	L	13
Parameters of relaxing	D_0	0.01
Parameters of annihilation	S_0	0.25
Parameters of disintegration	β_0	0.01
Parameters of turbulence	E_0	10^{-4}
Scaling parameters (χ,q)		1.5
Scaling parameters $(\delta,\sigma,b,\varepsilon,g,\mu)$		0.9

Intensity of the secondary magnetic field

All vortices of level l existing at time t make a similar contribution to the intensity of the secondary magnetic field. As announced in Sec. II, the contribution of vortices of the first orientation is considered as positive, the contribution of vortices of the second orientation negative. The secondary magnetic field generated at time t is thus expressed as follows:

$$H(t)=H_0\sum_{l=1}^{L}(p_1(l,t)-p_2(l,t))\chi^l, \tag{11}$$

where $p_i(l,t)$ denotes the density of vortices of ith orientation at level l at time t.

IV. MODEL BEHAVIOR

The model displays a very complex behavior. In the present work we will focus on the features which can be considered as symmetry breakings and might contribute to the understanding of the origin of the large scale geomagnetic field and of the occurrence of its polarity reversals.

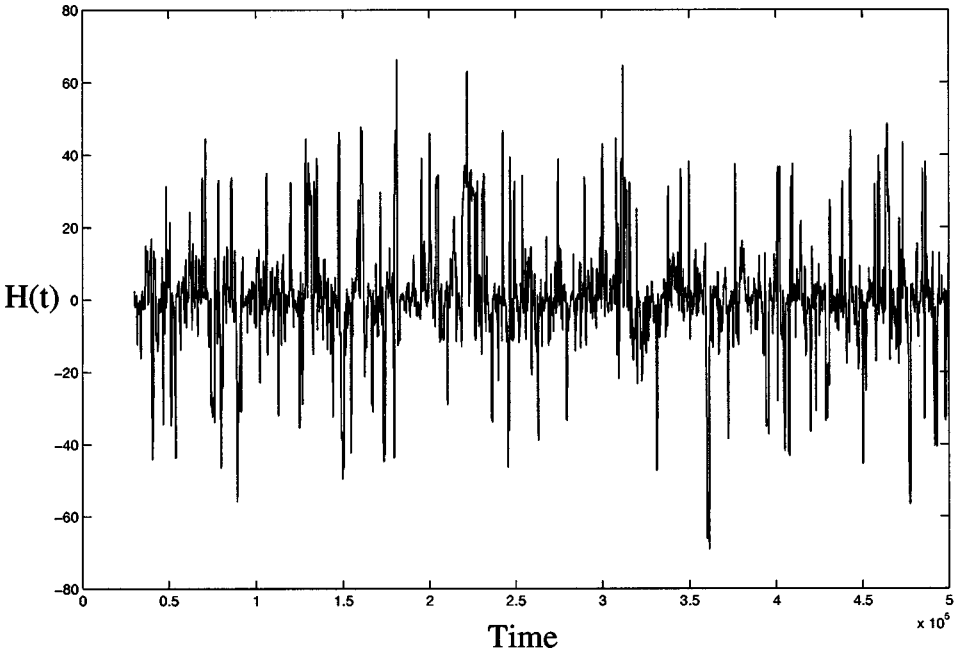

FIG. 9. Temporal evolution of the generated magnetic field intensity when the amplification effect of both the direct and inverse cascades is zero: $F_0=\alpha_0=\gamma_0=0$. See other parameters of the modeling in Table I.

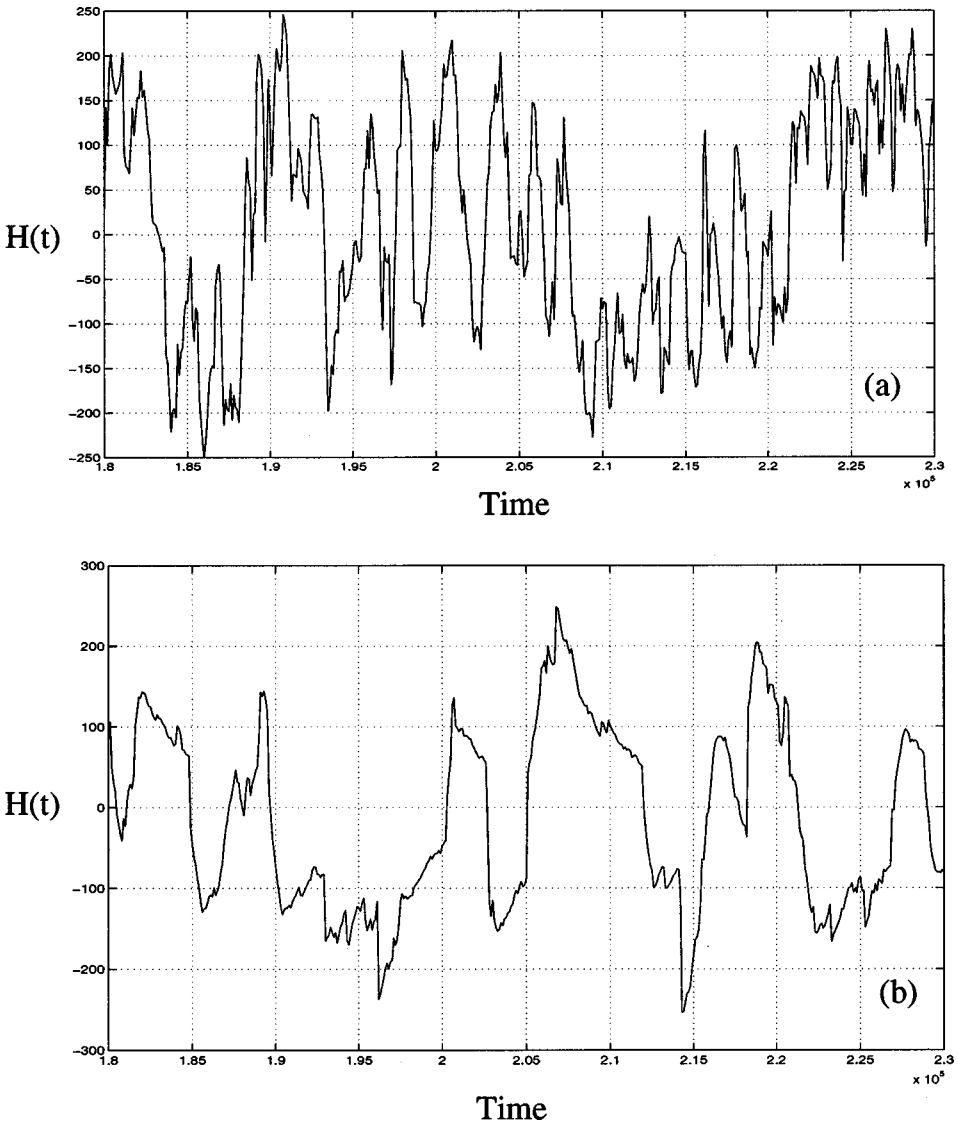

FIG. 10. Temporal evolution of the generated magnetic field intensity, when the amplification effect of the direct cascade is zero ($F_0=0$), for different parameters of the inverse cascade: (a) $\alpha_0=0.5$, $\gamma_0=0.5$; (b) $\alpha_0=0.99$, $\gamma_0=0.99$. See other parameters of the modeling in Table I.

A. Choice of parameters

We have introduced quite general equations to describe the evolution of the system; this approach allows us to keep open a wide field of possible applications of the model. However in the present paper we consider only a few free parameters, the majority of them being fixed (see Table I). We assume that the dynamics of vortices is characterized by the same scaling for all the involved processes (coupling, disintegration, relaxing, ...), i.e., by the same value of parameters $\delta,\sigma,b,\varepsilon,g,\mu$. The lifetime of vortices increases with their dimension, i.e., with the scale level; we therefore take the common value of the above scaling parameter, say ψ, less than unity. And, as we do not want too large a difference between two consecutive levels, we take $\psi=0.9$. On the other hand, the contribution of the disintegrated vortices to the direct cascade, as well as the contribution of all vortices to the magnetic field H [Eq. (11)] increase with their size. So, we take $q=\chi=1.5$.

We also consider that the influence of direct injection of turbulence is small in regard to the lifetime of vortices; the value of E_0 [Eq. (5)], characterizing the appearance frequency of turbulent vortices, is taken as 10^{-4}, whereas the parameter governing the lifetime is two orders of magnitude larger [$D_0=10^{-2}$, $\beta_0=10^{-2}$ see Eqs. (1) and (3)].

We have no reason to consider different durations for the two lifestates (strong and weak) of vortices; therefore we take $D_0=\beta_0$ [Eqs. (1) and (3)].

All the model parameters are then fixed, except for the ones characterizing the coupling probability [α_0, and γ_0, Eqs. (8) and (9)] and the intensity of the direct cascade [F_0, Eq. (5)]. In the following we investigate the model behavior in function of the strength of the direct and inverse cascades mechanisms.

In short, for the aim of the present study, we keep only three free parameters (F_0,α_0,γ_0). It will remain possible to extend the study by varying other parameters.

B. Symmetry breaking

We are interested in the possibility for the system to produce large scale symmetry breakings. These symmetry breakings will be characterized by two features: the duration of the intervals of constant polarity of the secondary magnetic field, and the intensity of this field. We will also compare the average duration of these constant polarity intervals with the characteristic time needed to change polarity.

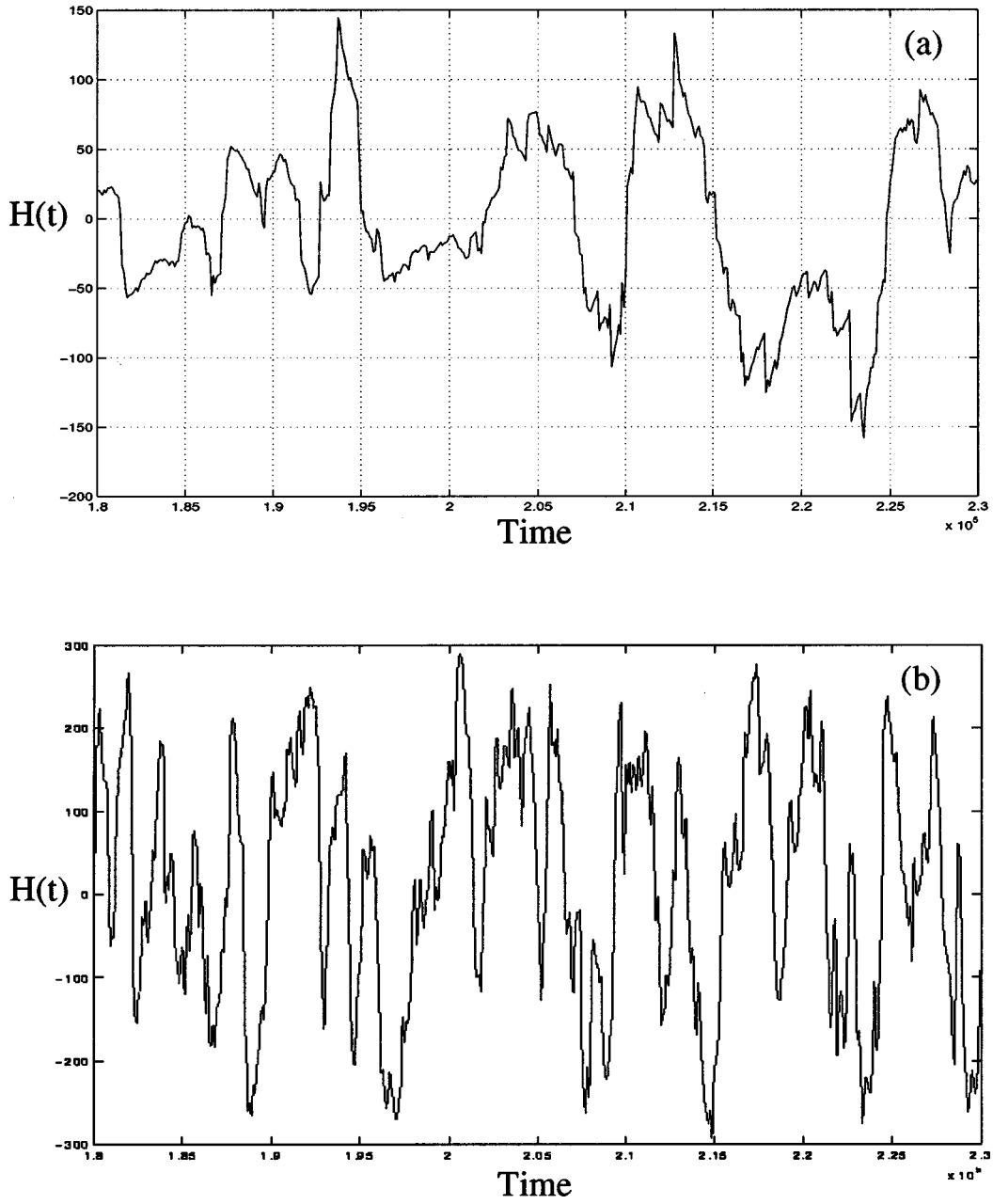

FIG. 11. Temporal evolution of the generated magnetic field intensity, when the amplification effect of inverse cascade is zero ($\alpha_0 = \gamma_0 = 0$), for different parameters of the direct cascade: (a) $F_0 = 1$; (b) $F_0 = 20$. See other parameters of the modeling in Table I.

The effect of the inverse cascade

Let us first investigate the effect of the inverse cascade of appearance alone [there is no direct cascade of appearance: $F_0 = 0$ in Eq. (5)]. If the coupling probabilities α_0 and γ_0 [Eqs. (8) and (9)] are close to zero, there are only small and short-duration symmetry breakings related to the random fluctuations of the turbulent flow (Fig. 9). When coupling probabilities α_0 and γ_0 increase, the amplitudes and durations of the symmetry breakings increase [Fig. 10(a)]. The maximum value of the magnetic field intensity is determined by the total volume of the system and the value of the scaling parameter χ. It may be reached if the coupling probabilities are large enough [Fig. 10(b)]. The average duration of constant polarity intervals cannot exceed a maximal value determined by the lifetime of the highest range vortices. It is thus impossible to obtain long intervals of constant polarity, even if the coupling probabilities are close to unity [Fig. 10(b)].

Remark: No physical unit has been introduced *a priori* in our abstract model. But, to calibrate the time scale, one can consider that the mean duration of the polarity intervals of Fig. 12 is, say, 3×10^5 yr; and, to calibrate the H (ordinate) axis, it is enough to consider that the maximum value which H can reach ($H_0 = \Sigma_l \chi^l$) is, say, 10^{-4} T.

The effects of the direct cascade

Let us now investigate the effect of the direct cascade alone; there is no inverse cascade and the coupling probabilities α_0 and γ_0 are zero. As the disintegration parameter F_0

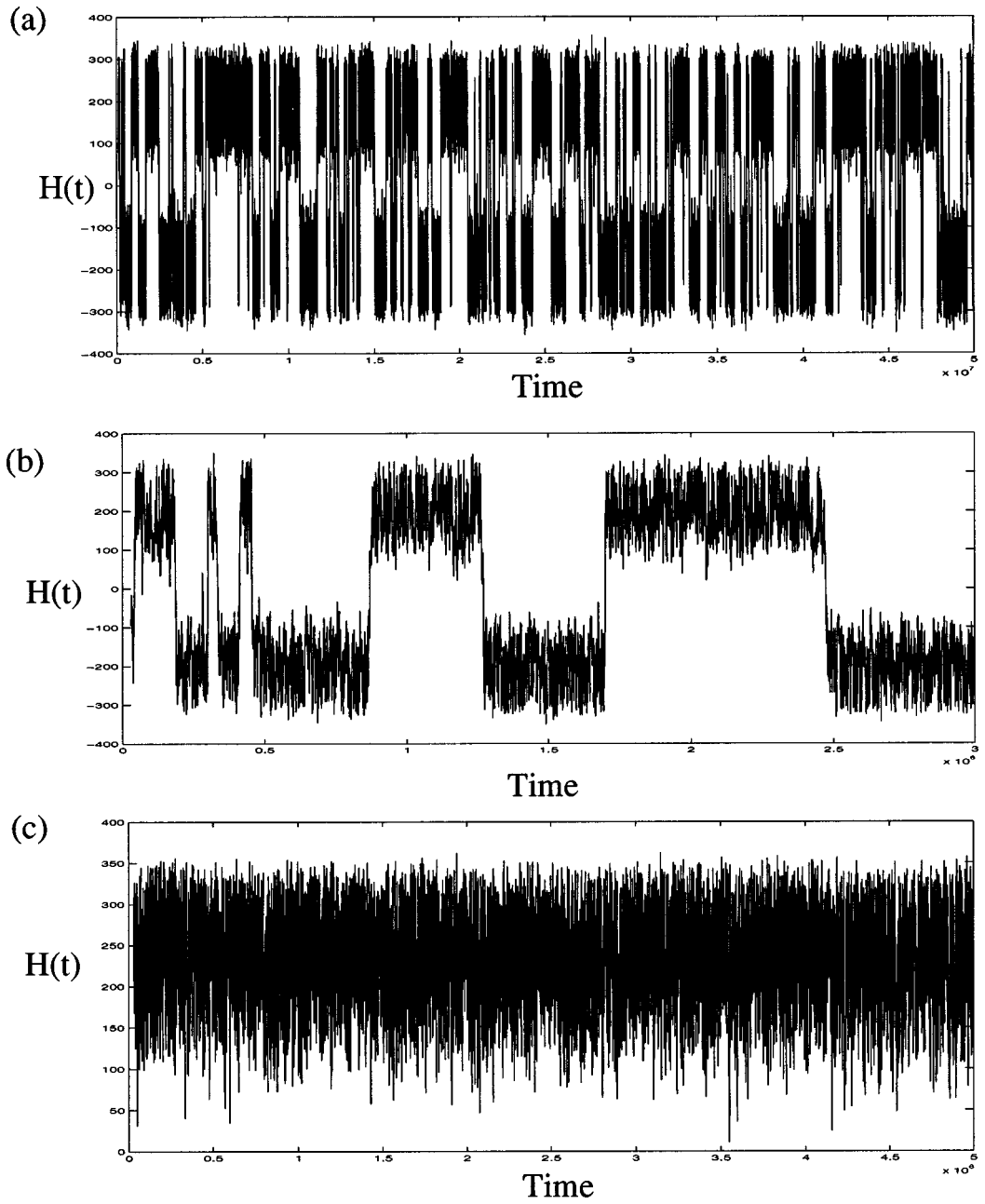

FIG. 12. Temporal evolution of the generated magnetic field intensity for a two-side cascade effect. (b) is a zoom of the first part of (a). Parameters of cascades: (a), (b) $F_0=0.5$, $\alpha_0=0.1$, $\gamma_0=0.01$; (c) $F_0=0.3$, $\alpha_0=0.2$, $\gamma_0=0.01$. See other parameters of the modeling in Table I.

grows [Eq. (5)], amplitudes and durations of the symmetry breakings increase [compare Fig. 9 and Fig. 11(a)]. Maximal values of the magnetic field intensity are achieved for large values of the disintegration parameter F_0 [Fig. 11(b)]; the average duration of constant polarity intervals is of the same order as in the case of the strong pure inverse cascade [see Figs. 10(b) and 11(b)]. Thus, in the case of a pure direct cascade alone, it is also impossible to obtain long lived symmetry breakings.

The physical meaning of a large value of the disintegration parameter F_0 is arguable; in this case indeed an unreasonable increase of the helicity flow appears when high level vortices are destroyed; conditions of such an increase should be discussed for each particular system. If reasonable values of F_0 are considered, only low values of the magnetic field intensity can be achieved, and the durations of polarity intervals are of the same order as the polarity changes (reversals) durations.

The up and down cascade effect

In contrast with the cases of one-sided cascades considered above, the interaction of both inverse and direct cascades produces strong and long symmetry breakings for relatively small values of the coupling and disintegration parameters [Fig. 12(a)]. The duration of constant polarity intervals is no longer directly limited by the lifetime of the vortices, and can be arbitrary large [Fig. 12(c)]. The maxi-

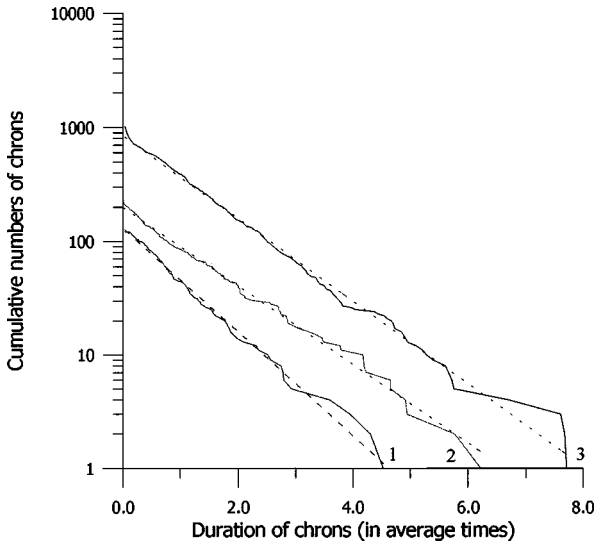

FIG. 13. The cumulative number of chrons vs its duration for real data (1), two-side cascade modeling (2), and pure direct cascade modeling (3). All curves are approximated by the exponential law (dashed straight lines) with similar slopes: (1) 1.05, (2) 0.79, and (3) 0.83.

mum possible value of the intensity of the secondary field is reached. The polarity reversals are completed in a very short time compared with the duration of the corresponding constant polarity intervals [Fig. 12(b)].

C. Properties of polarity intervals and reversals

If both cascades are operating, there is a domain of parameters for which high range long lived symmetry breakings are observed, as illustrated by Fig. 12. The distribution of the lengths of the constant polarity intervals, which we will call chrons as in the case of the geomagnetic field, is then exponential (Fig. 13, curve 2). But a similar trend can also be obtained in the case of a direct cascade alone (Fig. 13, curve 3).

It is also to be stressed that complex variations of the field generated by the model are observed during constant polarity intervals (Fig. 13), as in the case of the actual field. The detailed characteristics of these variations can be changed by changing the model parameters.

V. DISCUSSION AND CONCLUSIONS

Large scale symmetry breakings occur in various physical systems. In most geodynamo models, the α effect is supposed asymmetric *a priori*, the lack of mirror symmetry being attributed to Earth's rotation. The present work describes a way to obtain large scale and long lived symmetry breakings in a symmetric model of multiscale turbulent vortices. It has been shown that this kind of symmetry breaking results from an up and down cascade of energy transfer; it cannot be obtained in the case of a direct cascade alone, neither in the case of an inverse cascade alone. The cascade mechanism can amplify a primary magnetic field (this is why we call our model a dynamo model). In the case of one-sided cascades working alone (direct or inverse), this amplification needs large values of the cascades parameters (α, γ, or F_0). In the case of an up and down cascade, only moderate values of these parameters are needed to obtain a large scale perturbation from small values of the turbulent intensity.

The comparison of the behavior of our model with the behavior of the actual geomagnetic field is certainly excessive, at the present time, since our model is not a self-excited dynamo model A primary field H_0 is given, and we look at the behavior of the secondary field $H(t)$ generated from H_0, given by Eq. (11). $H(t)$ is strictly the amount of secondary field generated at time t during a time step; it would be the secondary field itself in the limit case of strong diffusion; the amplification $H(t)/H_0$ [Eq. (11)] is meaningless since no reaction of H on the flow is considered. But the multiscale turbulent mechanism studied here can be considered as an ingredient of a self-excited dynamo model, as in [20], and the next step of our work will indeed be to close the system by introducing diffusion and reaction of the magnetic field on the flow. The behavior of the submodel considered here, with its large scale and long lived symmetry breakings, will be retrieved in the complete model.

As said in the Introduction, the magnetic field of the Earth has reversed a large number of times during the geological history. The durations of the polarity intervals (chrons) are much larger than the durations of the reversals. The distribution of the chrons lengths obeys an exponential law [37] (Fig. 13, curve 1). During polarity intervals, the geomagnetic field presents complex time variations, with different time scales (paleomagnetic data essentially show the variation of the dipolar field). As shown in Sec. IV C, the secondary field generated by our model shares all these features. In future work we will further investigate the characteristics of the variations of the model during polarity intervals. It has been shown that the exponential distribution of chrons lengths is too rough a feature to really characterize the different kinds of symmetry breaking. It is more promising to study the relation between durations of chrons and durations of reversals (which appears to be specific in the case of the actual geomagnetic field) in order to get a measure of the different kinds of symmetry breaking.

Independently of these comparisons with an actual planetary magnetic field, we think that our simplistic hierarchical model of turbulence is worth considering by itself. In particular, the result that the system can present large scale and long lived symmetry breakings (in the form of periods of constant sign of a parameter H characterizing some large scale organization of the system) might be of general interest.

ACKNOWLEDGMENTS

The present work was completed in IPG, Paris while E. Blanter and M. Shnirman received a scientist visitation grant in the form of a IPGP/MITPAN Cooperation Agreement. The present work was also supported by the Russian Foundation of Fundamental Research (Project No. 96-05-65710), and by the INTAS Foundation (Project No. INTAS-93-457-ext).

[1] J. Bloxham and A. Jackson, J. Geophys. Res. **97**, 19 537 (1992).
[2] G. Hulot and J. L. LeMouël, Phys. Earth Planet. Inter. **82**, 167 (1994).
[3] L. Hongre, G. Hulot, and A. Khoklov, Phys. Earth Planet. Inter. **106**, 311 (1998).
[4] R. T. Merrill, M. W. McElhinny, and P. L. McFadden, *The Magnetic Field of the Earth* (Academic, San Diego, 1996).
[5] E. N. Parker, Astrophys. J. **122**, 293 (1955).
[6] F. Krause and K. H. Rädler, *Ergebnisse des Plasmaphysik und der Gaselektronik. Bd. II*, edited by R. Rompe and M. Steenbeck (Akademie-Verlag, Berlin, 1971), p. 1.
[7] F. Krause and K. H. Rädler, *Mean-field Magnetohydrodynamics and Dynamo Theory* (Pergamon Press, Great Britain, 1980).
[8] S. I. Braginsky, Geomagn. Aeron. **18**, 225 (1978).
[9] S. I. Braginsky and P. H. Roberts, Geophys. Astrophys. Fluid Dyn. **38**, 327 (1987).
[10] C. F. Barenghi, Geophys. Astrophys. Fluid Dyn. **60**, 211 (1991).
[11] R. Hollerbach, C. F. Barenghi, and C. A. Jones, Geophys. Astrophys. Fluid Dyn. **67**, 1 (1992).
[12] C. F. Barenghi, Geophys. Astrophys. Fluid Dyn. **67**, 27 (1992).
[13] D. Jault, Geophys. Astrophys. Fluid Dyn. **79**, 99 (1995).
[14] G. A. Glatzmaier and P. H. Roberts, Nature (London) **77**, 203 (1995).
[15] W. Kuang and J. Bloxham, Nature (London) **389**, 371 (1997).
[16] L. R. Richardson, *Weather Prediction by Numerical Process* (Cambridge University Press, Cambridge, England, 1922).
[17] E. A. Novikov and R. W. Stewart, Izv. Akad. Nauk SSSR, Ser. Geoffiz. **9**, 408 (1964).
[18] U. Frisch, *Turbulence, the Legacy of A. N. Kolmogorov* (Cambridge University Press, Great Britain, 1995).
[19] A. N. Kolmogorov, Dokl. Akad. Nauk SSSR **30**, 9 (1941); reprinted in [Proc. R. Soc. London, Ser. A **434**, 9 (1991)]; A. N. Kolmogorov, Dokl. Akad. Nauk SSSR **31**, 538 (1941); A. N. Kolmogorov, Dokl. Akad. Nauk SSSR **32**, 16 (1941) [Proc. R. Soc. London, Ser. A **434**, 15 (1991)].
[20] J.-L. Le Mouël, C. J. Allègre, and C. Narteau, Proc. Natl. Acad. Sci. USA **94**, 5510 (1997).
[21] C. J. Allègre, J. L. Le Mouël, and A. Provost, Nature (London) **297**, 47 (1982).
[22] C. J. Allègre and J.-L. Le Mouël, Phys. Earth Planet. Inter. **87**, 85 (1994).
[23] C. J. Allègre, J.-L. Le Mouël, H. D. Chau, and C. Narteau, Phys. Earth Planet. Inter. **92**, 215 (1995).
[24] E. M. Blanter, M. G. Shnirman, J.-L. Le Mouël, and C. J. Allègre, Phys. Earth Planet. Inter. **99**, 295 (1997).
[25] E. M. Blanter, M. G. Shnirman, and J.-L. Le Mouël, Phys. Earth Planet. Inter. **103**, 135 (1998).
[26] E. M. Blanter and M. G. Shnirman, Phys. Rev. E **53**, 3408 (1996).
[27] G. S. Narkunskaya and M. G. Shnirman, Phys. Earth Planet. Inter. **61**, 29 (1990).
[28] A. J. Chorin and J. Marsden, *A Mathematical Introduction to Fluid Mechanics* (Springer, New York, 1993).
[29] A. J. Chorin, *Vorticity and Turbulence* (Springer, New York, 1994).
[30] P. S. Marcus, J. Fluid Mech. **215**, 393 (1990).
[31] P. H. Roberts, Mathematika **19**, 169 (1972).
[32] V. I. Oseledets, Russ. Math. Surv. **44**, 210 (1989).
[33] J. Marsden and A. Weinstein, Physica D **7**, 305 (1983).
[34] D. Montgomery, L. Phillips, and M. L. Theobald, Phys. Rev. A **40**, 1515 (1989).
[35] J. P. Dahlburg, D. Montgomery, G. D. Doolen, and L. Turner, Phys. Rev. Lett. **57**, 428 (1986).
[36] X. Shan, D. Montgomery, and H. Chen, Phys. Rev. A **44**, 6800 (1991).
[37] S. C. Cande and D. V. Kent, J. Geophys. Res. **100**, 6093 (1995).